MULTI-FREQUENCY SYNTHESIS

J. E. CONWAY
Owens Valley Radio Observatory and Jet Propulsion Laboratory,
California Institute of Technology, Pasadena, CA 91125, U.S.A.

ABSTRACT   A method of improving image fidelity by using
observations at multiple frequencies is described. We discuss the power
and possible limitations of the technique. Results of narrow frequency
range observations with MERLIN and global VLBI are presented. We
conclude with a consideration of the possible future impact of this
technique.

INTRODUCTION

Aperture synthesis observations with sparse arrays usually have insufficient
data to fully constrain their output images, giving errors which limit our
astrophysical interpretation. Non-linear image reconstruction algorithms must
be applied which effectively interpolate from the measured uv data to estimate
unmeasured Fourier components. The larger the holes in the uv coverage,
or the more complex the image, the larger the 'reconstruction errors' which
result. In Multi-Frequency Synthesis observations are made at a number of
frequencies n_f over a 10% to 30% range. Changing frequency changes the
spatial frequency of the Fourier components that we measure. With MFS the
gaps in the uv coverage are much reduced (see Fig 1) and so we can obtain
higher fidelity images (Conway, Cornwell and Wilkinson 1990, which we will
refer to as CCW).
      The problem with this technique is that the source structure could
potentially vary dramatically with frequency. But in continuum sources
the spectrum at each pixel is fairly smooth, and the images at the different
frequencies are highly correlated, it is these facts which allow us to contemplate
using MFS. We find that the effects of frequency dependent structure are often
below the thermal noise, as explained below, and in these cases we can obtain
the full benefit of having n_f times more data. Even when spectral effects
exceed the thermal noise we find that they can usually be accounted for if we
parameterize the image in terms of two unknowns at each pixel; the intensity
at some average frequency and some form of frequency derivative. The use
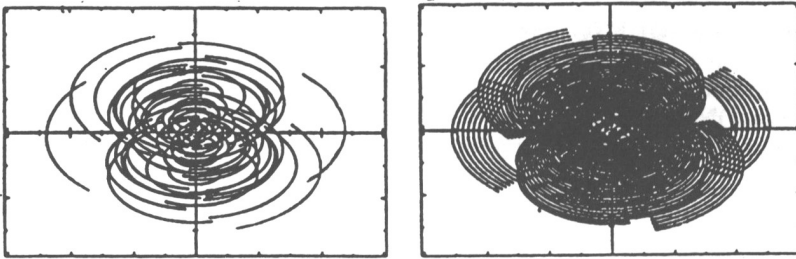of MFS then doubles the number of unknowns for which have to solve but we

Fig. 1.   Aperture coverages achievable with the full VLBA at declination 30°. Left: at a frequency of 1660 MHz. Right: Using MFS with 8 frequencies spread over 1350 – 1750 MHz.

have now n_f more observables. If n_f is greater than 2 the MFS image remains better constrained than the single frequency image.

SPECTRAL EFFECTS

We now consider the nature and size of the effects that arise on combining uv data at different frequencies. If all parts of a source had the same spectrum we could simply adjust the amplitudes at each frequency and then combine the data in the aperture plane, invert and deconvolve and there would be no spectral effects in the resulting image. Even when the spectrum varies across the source it is always worth removing some 'average' spectrum to reduce spectral effects. After rescaling the amplitude at each frequency by a factor $g(\nu)$ the data at frequency ν are the same as from a source of brightness distribution $I'(x,y,\nu) = I(x,y,\nu)g(\nu)$. On combining all these data sets in the aperture plane and Fourier inverting the dirty map can be written as the following expansion

$$I'(x,y,\nu_o) * B_o \quad + \quad \left.\frac{dI'(x,y,\nu)}{df(\nu)}\right|_{\nu=\nu_o} * B_1 \quad + \quad \frac{1}{2}\left.\frac{d^2I'(x,y,\nu)}{df^2(\nu)}\right|_{\nu=\nu_o} * B_2 \ldots$$

where the symbol * denotes convolution and $f(\nu)$ is some function of frequency. The derivatives are functions of spatial coordinates x and y and will be referred to as 'coefficient images'. The B_n are generalised dirty beams which are the Fourier transforms of the MFS uv coverage with each uv point weighted according to its frequency of observation by $(f(\nu))^n$. In CCW we considered the common case where the spectrum at each pixel is, to good approximation, a power law with position dependent spectral index $\alpha(x,y)$ so that $I(x,y,\nu) = I(x,y,\nu_o)(\nu/\nu_o)^{-\alpha(x,y)}$. We assume that the amplitudes have been corrected for an 'overall' spectral index α_o so that $g(\nu) = (\nu/\nu_o)^{\alpha_o}$ and so $I' =$
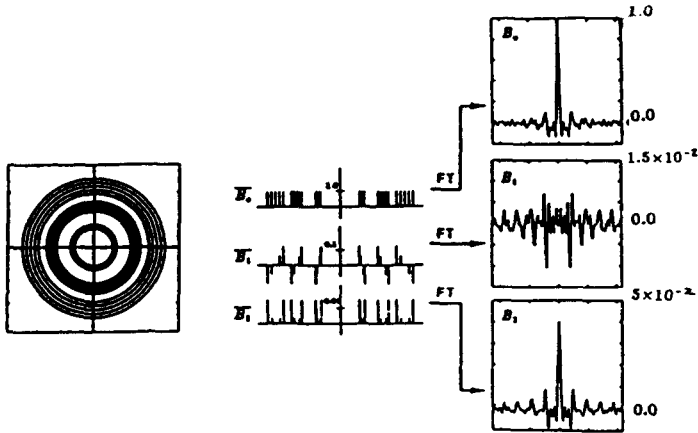
Fig. 2. Illustration of the nature of the spectral dirty beams. Left: A simple uv coverage formed from 3 antennas and 5 frequencies. Middle: A slice across the uv coverage showing the weightings corresponding to different order of spectral dirty beam. Right: Slices through the beams formed from Fourier transforming the weighted coverages.

$I(x, y, \nu_o)(\nu/\nu_o)^{-\alpha'}$ where the residual spectral index $\alpha'(x, y) = \alpha - \alpha_o$. We can expand in any form for $f(\nu)$ that we wish; for the case of power law spectra the choice $f(\nu) = \ln(\nu_o/\nu)$ is appropriate. The general expansion for the dirty map becomes

$$I(x, y, \nu_o) * B_o \quad + \quad I(x, y)\alpha'(x, y) * B_1 \quad + \quad \frac{1}{2}I(x, y)\alpha'^2(x, y) * B_2 \ldots$$

Fig 2, illustrates the nature of the spectral dirty beams for a simple example uv coverage. Note that there is a clear difference between the even and odd order dirty beams, the former have large central lobes whilst the latter have no such central peak. In CCW it was shown that that the peak sidelobes due to B_1 are of the order of 5×10^{-3} for aperture coverages typical of VLBI arrays and a frequency range of about 25 %. We can often choose α_o such that α' is about 0.1 or 0.2 in the brightest regions, so that the spectral errors can occur at levels of between $I/1000$ and $I/2000$, i.e. at dynamic ranges of a 1000 or so. For images with dynamic ranges below this level we can usually ignore the contributions due to spectral effects.

DOUBLE DECONVOLUTION

Even if spectral effects are important, the dirty map can usually, within the noise, be described by the first two terms of the Taylor expansion. In such situations we need an algorithm which solves for both the $I(x, y)$ and $I\alpha'(x, y)$ coefficient images. Various approaches to this problem have been investigated (Conway 1988). One promising approach, Double Deconvolution (DD), is

an iterative algorithm which alternately attempts to estimate the I and $I\alpha'$
distributions. It does this by convolving the map alternately with each of the
two spectral dirty beams, B_0 and B_1. and then CLEANing the result with
the appropriate dirty beam. The algorithm is explicitly based on the original
description of CLEAN (Högbom 1974) as a beam recognition algorithm. For
further details we refer the reader to CCW.

Figure 3 illustrates the effectiveness of the algorithm with simulated
data. Fig 3a shows the model image. Fig 3b shows the reconstruction obtained
on CLEANing conventional single frequency data; it is badly affected by
reconstruction errors. Fig 3c shows the effect of simply combining the data sets
reweighting, inverting and deconvolving. The ring-like 'spectral errors' are the
contribution of the $I\alpha' * B_1$ term in the expansion for the dirty map. Fig 3d
shows the result of applying two cycles of Double Deconvolution. The spectral
errors are removed and a good reconstruction is achieved.

As in CLEAN, it can be shown that DD is guaranteed to converge to fit
the data. In situations in which the number of independent observables is more
than double the number of filled pixels in the image, convergence to fit the
data should give an image that is unique and true within the noise. To be well
conditioned with respect to noise the fractional frequency ranges must span
the gaps in the uv coverage; in fact some overlap between different physical
baselines at different frequencies will be required. Such situations are feasible
for some practical implementations of MFS, giving rise to the promise of
almost unique images in such cases. More often, however, despite MFS, there
will still be fewer constraints than unknowns. However, a successful separation
between the effects of I and $I\alpha'$ using DD is still possible, because to achieve
separation the algorithm implicitly uses the *a priori* information that the I and
$I\alpha'$ distributions are compact. Futhermore it can be shown (Conway 1988) that
if we switch from CLEANing one distribution to CLEANing the other before
the residuals are dominated by the sidelobe effects of the distribution for which
we are not CLEANing then progress toward a correct separation continues. In
practice this means we should switch our CLEANing when the sidelobe levels
in regions away from the source stop decreasing.

COMPLICATIONS - HIGHER ORDER TERMS

The DD algorithm assumes the dirty map can be expressed as a two order
expansion. At high dynamic range this assumption will break down as the
higher order terms become significant with respect to the thermal noise.
Because the second order beam is very similar to to the zeroth order beam
and has a central peak (see Fig 2), its main effect is to add a small bias to the
output image. The more important sidelobes which might obscure weak detail
are much smaller. We can rearrange the general expansion to show that the
dirty map equals

$$\left[I'(x,y,\nu_o) + B_2(0).\frac{1}{2}\frac{d^2 I'(x,y,\nu)}{df^2(\nu)} \right] * B_0 + \frac{dI'(x,y,\nu)}{df(\nu)} * B_1 + \frac{1}{2}\frac{d^2 I'(x,y,\nu)}{df^2(\nu)} * B_2'$$

evaluated at $\nu = \nu_o$. In this expression $B_2' = (B_2 - B_2(0).B_0)$ and $B_2(0)$ is
the central value of the second order beam (which for a 25 % frequency range
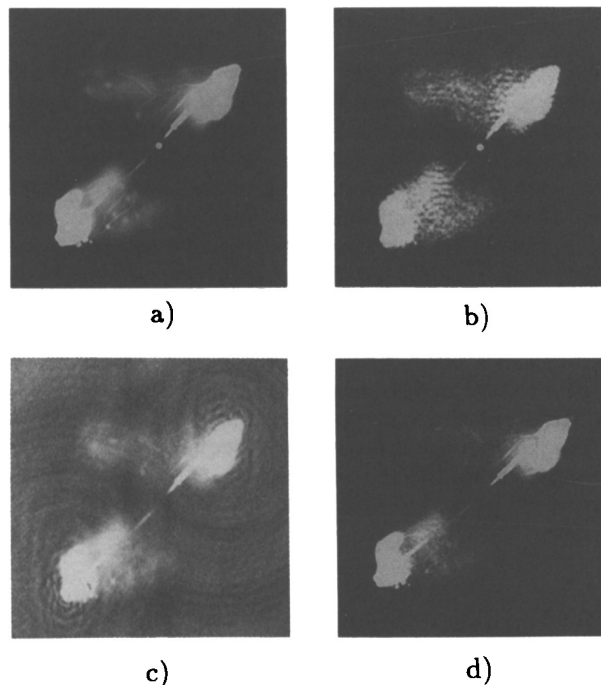
Fig. 3. Applying Double Deconvolution to Simulated data. a) The model intensity distribution. b) The results of mapping single frequency data. c) The results of combining and deconvolving multi- frequency data. d) After applying two cycles of Double Deconvolution.

is about 1/200). If we assume a two order expansion and apply DD we would obtain an I image biased by $B_2(0)$ times the second derivative of I with respect to $f(\nu)$. In practice the bias on source will always be < 1%. It will be strongly correlated with intensity variations and so is unlikely to mask weak detail or be astrophysically important. If we accept this bias the effective second order dirty beam equals $(B_2 - B_2(0).B_0)$. This is very similar to the B_1 beam in having no central peak, only weak sidelobes. For a 25 % frequency range these sidelobes are at the 5×10^{-4} level (a figure which scales as the square of the frequency range).

The second order term that arises from a pure power law spectra $(I\alpha'^2/2)$ will be very small. For a hotspot with $\alpha' = 0.2$ the effective second order spectral sidelobes occurs at the 10^{-5} level. Even these small effects can potentially be removed by using the (slightly biased) estimates for I and $I\alpha'$ from DD to estimate and remove the $I\alpha'^2$ terms. An iterative process should be able to estimate of I and α almost exactly (Cornwell 1984). More generally the spectra are affected by synchrotron self-absorption or electron aging which give second order derivatives which cannot be derived from the lower derivatives. One important case occurs in imaging core-dominated sources. Usually the unresolved core has a slightly curved spectrum. One way to reduce the second order effects in this case is to rescale the amplitude at each frequency by $g(\nu) = 1/S(\nu)$ where $S(\nu)$ is the total flux of the source at

frequency ν. This effectively removes the curvature in the spectrum of the brightest 'core' component and transfers it into the effective spectra of the much weaker secondary components, which will have much smaller second order spectral spectral errors. The most challenging situation for MFS occurs in cm wavelength global VLBI, in which the image often contains several spatially resolved self-absorbed components which peak at different frequencies. For the source NRAO140 the spectra of the multiple components within the jet have been determined (Marscher 1988). If MFS observations of this source with the VLBA plus Bonn were made in L-band with a 25% frequency range simulations show that the effective second order effects would be dominated by a single component which peaks near the observing band, giving peak second order sidelobes at 5×10^{-4} of the peak intensity. Fortunately in this source and others significant curvature at the observing frequency is limited to only a small part of the jet. We could image each frequency separately and estimate the spectral curvature within that small region. After removing the effects of this spectral curvature from the MFS data we can obtain much higher dynamic range MFS images.

COMPLICATIONS - SELF CALIBRATION

Although by using n_f frequencies we can make the uv coverage equivalent to that obtained by an array with $\sqrt{n_f}$ times as many telescopes it will not be equivalent in the number of phase closure constraints. If self-calibration is done at each frequency separately the ultimate fidelity of our MFS map may be limited by 'self-calibration errors' which depend on the single frequency aperture coverages. No matter how well MFS fills the plane there will only be a statistical improvement on combining the data sets.

One way to improve things is to use the output I and $I\alpha'$ from DD to generate model images at each of the frequencies, and then to use these model images in separate self-calibrations at each frequency. The corrected data could be used as input for a new DD cycle and so on iteratively. This method at least indirectly uses the information at all the frequencies to constrain the self-calibration solution. Much more can be done if the multi-frequency data are collected simultaneously or almost simultaneously (by rapid frequency switching) at the different frequencies. We can use the fact that the antenna-based phase errors are highly correlated to constrain our self-calibration solutions. In principle we need only solve at each antenna for a delay term (phase $\propto \nu$) and at low frequencies an ionospheric term (phase $\propto 1/\nu$). Determining the phase error at each antenna absolutely from the frequency dependence of phase is likely to be badly conditioned with respect to noise. More practically we might solve at each antenna for a phase error at an average frequency plus a linear gradient in frequency plus higher terms (if the ionospheric is significant). If we have only two unknowns for each of the N antennas then the ratio of constraints (uv points) to unknowns (source visibilities plus antenna phase parameters) is approximately $n_f N/(n_f N + 4)$; for high enough n_f this ratio can exceed that for an 'equivalent coverage' single frequency array which is $\sqrt{n_f} N/(\sqrt{n_f} N + 2)$.
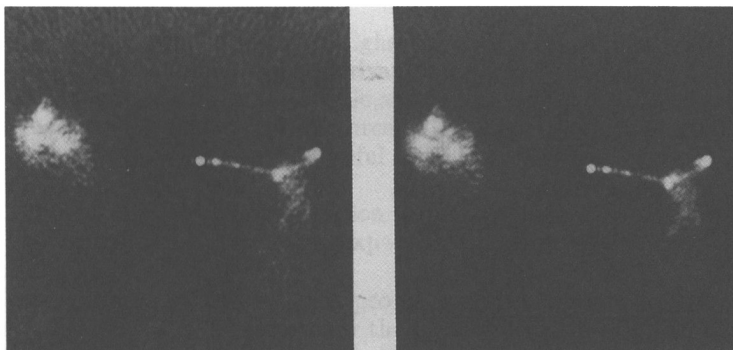
Fig. 4.   Results of MFS mapping with MERLIN of the complex
source 3C179 at L -band. Left: the best single frequency map. Right:
MFS map made from five frequencies over 7%.

OBSERVATIONAL RESULTS

We briefly describe the results of two observational tests of the MFS technique.
In both cases the achieved frequency ranges were rather small (< 8 %), and
insufficient to reach across the gaps in the single frequency aperture coverage.
Simulations suggest that in such cases the improvements in fidelity can be
useful, but not as dramatic as that which can be seen by contrasting Fig 3b
and 3d. In both tests the fractional spectral dirty beam sidelobes and the
required dynamic range were such that the expected spectral errors were below
the noise level and there was no need to use the DD algorithm.
      Observations of the complex high declination source 3C179 were made
at 5 frequencies in L-band (1612, 1632, 1662, 1690 and 1720 MHz) with the
MERLIN array. Each of the frequencies was observed on a different day.
The data at each frequency were separately mapped and self-calibrated. The
amplitudes at each frequency were rescaled by a spectral index of 0.5 and then
the data were combined in the uv plane together with a single snapshot of VLA
A-array data. The resulting image after inversion and CLEANing is shown in
Fig 4 together with the best single frequency image (at 1632 MHz). There are
small but clear improvements, especially in the removal of the striping effect in
parts of the western lobe.
      In September 1989 global VLBI observations of the source 3C84 were
made at frequencies of 21.7, 22.2 and 23.5 GHz, again on separate days. This
target and frequency band were chosen for the first MFS VLBI observations
because even at low dynamic range (less than 100:1) the structure was too
complex to be constrained by the available single frequency aperture coverages.
To date the middle and higher frequency have been successfully fringe-fitted,
self-calibrated, combined, inverted and CLEANed to give the provisional map
of the inner few parsecs shown in Fig 5. On going from a single frequency to
two frequencies the dynamic range of our image improved almost immediately
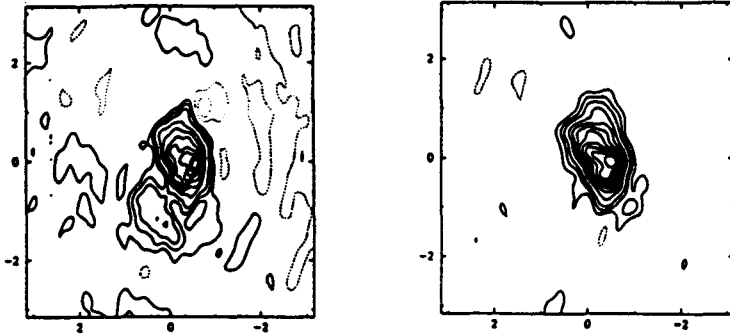by a factor of 3. Processing of the MFS data is continuing.

Fig. 5. Results of MFS mapping with Global VLBI of the nuclear region of 3C84 at K-band. Left: the best single frequency map. Right: MFS map made from two frequencies separated by 5%. Contour levels at $-2, 2, 5, 10, 20...100$ %. Restoring beam is 0.3 mas circular.

FUTURE IMPACT

The MFS technique has an important role to play in improving the fidelity of images produced from sparse arrays such as the VLBA/Global VLBI, MERLIN and the AT. With the advent of the VLBA the complexity of VLBI images will no doubt dramatically increase as high sensitivity systems are regularly used to observe some of the brightest sources. At the same time the number of antennas available will not be dramatically increasing. Fortunately the VLBA is in a good position to exploit MFS. Unlike most present VLBI antennas it can tune over a wide frequency range so that at most bands it can cross most of the gaps in the single frequency uv coverage. Furthermore it can observe up to 8 frequencies simultaneously over about 400 MHz allowing multi-frequency self-calibration. More frequencies can be added by switching the LO frequency. The Australia Telescope is also well designed for MFS; full aperture coverage can normally only be achieved by moving the antennas, but by using MFS the speed and versatility of the instrument can be greatly improved.

REFERENCES

Conway, J. E. 1988. *PhD Thesis, University of Manchester.*
Conway, J. E., Cornwell. T.J. and Wilkinson, P.N. 1990. *M..V.R.A.S.*, **246**, 490.
Cornwell, T. J. 1984. *VLBA Memo No 324.*
Högbom, J. A. 1974. *Astr. Ap. Suppl.*, **15**, 417.
Marscher, A. P., 1988. *Ap. J.*, **334**, 552.

Ray Norris: Have you considered using a two-parameter model to account for complex source spectra, allowing very wide bandwidths (e.g. octaves) to be used?

John Conway: Clearly for the very highest dynamic range or octave bandspread such a fit to the higher derivative coefficient images would be useful. I doubt however that any simple adaptation to Double Deconvolution could be made which could solve for three unknowns per pixel. A MEM based algorithm would probably be more useful for this problem.

David Murphy: An obvious application for Multi-Frequency Synthesis is space VLBI. What benefits could we expect to gain and what would be the limitations?

John Conway: In order to greatly improve fidelity it is important to cross the gaps in the uv-plane. The holes for the proposed space VLBI missions are (at least) octave sized, frequency ranges of < 30% may be useful, but will not give a really dramatic improvement. With octave frequency ranges we have all the problems of spectral curvature and higher derivatives. Multi-frequency modifying using synchrotron self-absorbed components may however be a good approach to deriving physical parameters and morphology from multi-frequency uv data.